

Towards Bi-Material 3D Printed Soft Microrobots using Two-Photon Polymerisation

Mehdi Salah^{1*}, Yannis Bordes¹, Cédric Clévy¹, Gwenn Ulliac¹,
Vincent Luzet¹, Adam Chafai², Muamer Kadic¹,
Pierre Lambert², Kanty Rabenoroso^{1*}

^{1*}FEMTO-ST Institute, Univ. Bourgogne Franche-Comté, UMR CNRS
6174, 15B avenue des Montboucons, Besançon, 25030, France.

²Transferts Interfaces and Processes (TIPs), Université Libre de
Bruxelles, Av. Franklin Roosevelt 50, Brussels, B-1050, Belgium.

*Corresponding author(s). E-mail(s): mehdi.salah@femto-st.fr;
kanty.rabenoroso@femto-st.fr;

Contributing authors: yannis.bordes@femto-st.fr; cedric.clevy@femto-st.fr;
gwenn.ulliac@femto-st.fr; vincent.luzet@femto-st.fr;
adam.chafai@ulb.be; muamer.kadic@femto-st.fr; pierre.lambert@ulb.be;

Abstract

2-Photon Polymerization (2PP) 3D printing has allowed several interesting fabrication processing for microrobots. However, QUESTIONS. Toward this goal, we investigate the behavior of 3D 100 μm -scale tethered microrobots made with bi-material 2PP printing. Beams of pNIPAM are used as actuators into an IP-S flexible mechanism, which took the function of structural skeleton of the microrobots. The force and displacement capabilities of pNIPAM beams actuators are studied experimentally and through Finite Element Modelling (FEM), revealing promising capacities in displacement and forces (measured contraction up to 30%, force up to 166 μN). The behavior of pNIPAM-actuated IP-S flexible mechanisms is investigated. The angular movement of pNIPAM-actuated IP-S rotational beam joint with varying dimensions was studied, and showed a max joint rotation of 23°. Furthermore, a repeatable 80 μm long motion was demonstrated on a 300 μm long RR robot mechanism during 5 actuation cycles. Last, actuated 3D mechanisms are demonstrated with three 100 μm grippers with two jaws oriented 45° around x , 45° around x and y , and three vertical jaws.

Keywords: Two-Photon Polymerization, Bi-material 3D printing, 4D Printing, Microrobots, Active materials, pNIPAM

1 INTRODUCTION

As more and more scientific and industrial interest is ported on micrometric objects, especially their assembly or their characterization, a need for robotic micromanipulation systems has arisen to control the movement and force applied by a tool on the object of interest [1], [2], [3]. However, classical robotic micromanipulation systems based on tools with micrometric size tips and commercially available positioning stages are limited by their decimetric scale (when considering their different components i.e. body of the robot and actuation systems) which heavily hinders the dexterity and positioning accuracy of their end-effectors at the micrometric scale. Reducing the size of the micromanipulator is interesting in order to access more constrained spaces and improving the robot's dexterity and precision. Especially, using a micromanipulator with embedded actuation could allow to apply forces in the μN to 100's of mN ranges, which can be useful for several applications [4], [5].

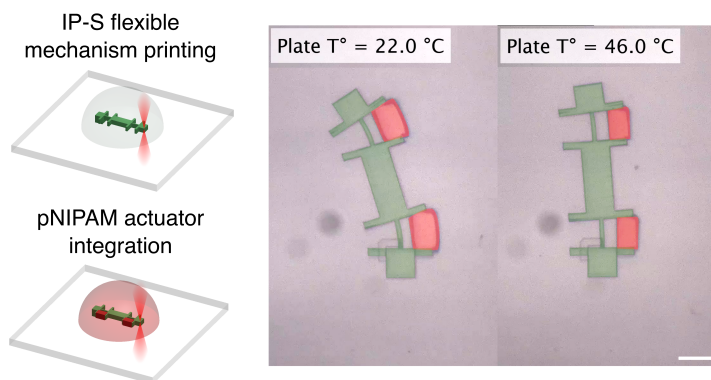


Fig. 1: 3D printed bi-material soft microrobot composed of a flexible mechanism in IP-S (highlighted in green) and two pNIPAM actuators (highlighted in red). We depict its actuation when heated at 22°C and 46°C. Scale bar: 50 μm .

To this end, researchers have explored micromanipulator designs at a smaller scale. Several manipulator have been proposed at the centimeter scale [6], [7], [8], [9], [10], demonstrating multi-Degree-Of-Freedom (multi-DOF) movement in a large workspace relatively to their size, paving the way for new tasks realization. While their size is centimetric, those examples illustrate that the scale down is not straightforward: each work had to propose a new way of building the robot to attain their size, such as using microlithography assembled with a small compliant Stewart platform [10], fabricate laminated devices [6], [7] or parallel continuum robot with glass legs [8].

The same need to propose other fabrication techniques arise at the millimeter scale and below. Several systems with embedded actuation and movement transformation

have been proposed, following various manufacturing approach like MEMS-based manufacturing [11] and Focused Ion Beam folding [12]. As a recent fabrication method, 2PP is a 3D printing technique capable of making μm -scale structures [13]. In particular, the use of active materials with 4D printing hold potential for several application fields [14] like microrobotics [15]. In addition, many 4D-printed devices use stimulus-responsive hydrogels, such as poly(N-isopropylacrylamide) (pNIPAM) based hydrogel or bovine serum albumin (BSA) based hydrogel, to generate movement, thanks to their important shrinkage when subjected to the appropriate stimulus.

In the micromanipulators case, 4D printing allow to create devices that deform themselves, which could then move an end-effector around their body. However, to generate meaningful movements beyond a simple shrinkage, an asymmetry in the deformation of the device need to be introduced [16], by using bilayer systems [17], [18], [19] or voxels-based designs [20] for example. To introduce asymmetry in 2PP printed devices, two ways have been mainly studied in the literature: Gray-tone Lithography (GTL) and multi-material printing. GTL modifies the material properties across the devices by locally tuning the printing parameters. This technique has demonstrated its interest in the state-of-the-art [19], [18], [21], [22],, but is limited by what is achievable with the base material. Each material parameters can only be tuned within a relatively small range (for example, the Young's modulus of pNIPAM in its swollen state can only be tuned in the 10's of kPa range [23]), and in the case of active materials, all the device will be stimuli-responsive : the deformation asymmetry is created bu tuning the amplitude of the response. Multi-material printing approaches are based on the use of multiple material in different parts of the devices to introduce asymmetry and various behaviors. Nishigushi et al. [24] and Zhang et al. [25] took advantage of a passive material lattice to control the movement of a bloc of active hydrogel, while Ozkäle et al. [26] printed a passive material around light-sensitive microactuators made in active materials. Especially, Ma et al. [27] demonstrated musculoskeletal systems made with a 2-step printing process in one chip, where a PH-responsive active hydrogel (bovine serum albumin or BSA) actuates a SU-8 compliant skeleton.

All these works have explored the fabrication of active microscale devices which integrate their actuation with 2PP 4D printing of active materials. However, the 2PP 4D printing process still need to be explored in the perspective of making micromanipulators. For micromanipulator, it is necessary to find ways to access the largest workspace possible with the smallest scale possible, generate multi-DoF movement in a controlable and repeatable manners, apply substantial forces, and how how to use 2PP 4D printing to respond to all these needs is still a wide open question in the state of the art.

A multi-material approach has several interesting features for the fabrication of micromanipulators. The use of two material allow to take advantage of huge stimuli-induced deformation difference and elastic modulus difference across the device (For example in [27], a maximal stimuli-induced deformation of 42 % in the BSA and 0%

in the SU-8, and elastic modulus of X kPa for the BSA and Y MPa for the SU-8), which could help to efficiently guide the deformation of the active material in a useful movement. It also allows to place the active material in specific locations, which could help the multi-DoF control of the microrobot. Moreover, the passive material can be used advantageously to make a stable structure for the robot capable to withstand and apply substantial forces. The use of a passive material with a simple mechanical behavior (for example a linear elastic material with no substantial sensibility to its environment) could also allow to make microrobots with a predictable and repeatable behavior.

To explore these possibilities, we investigated the use of IP-S, a passive material, with pNIPAM, a thermo-sensitive active hydrogel, in bi-material mechanisms with integrated actuation (Fig. 1) printed with 2-step 2PP printing. To the best of knowledge, bi-material tethered soft microrobots based on 2PP have never been proposed at 100 μm scale, with flexible mechanism structural skeleton, force and displacement analysis with repeated cycle and printing, and finally demonstrated on 3D microgrippers. The methods applied in this work are presented in section II. In section III, the static behavior of pNIPAM actuator and its capacity to produce large displacements and forces are studied through experimental measurement of free displacement and FEM simulation of displacement under load on 50 μm long pNIPAM beams considered as actuators. The impact of the printing speed on the pNIPAM actuators was also investigated according the maximal displacement and forces generated by the pNIPAM actuator. In section IV, the behavior of 100 μm -scale IP-S mechanism with integrated pNIPAM actuators is characterized. The angular movement of a beam rotational joint actuated by a pNIPAM actuator is studied in different configurations. The actuation of a 300 μm long RR microrobot mechanism is studied, with the repeatability of its movement tested during 5 actuation cycles. As a proof of concept for 3D actuated mechanisms, 100 μm -scale actuated grippers are fabricated and actuated. Finally, conclusion and perspectives close the paper.

2 METHODS

2.1 Design, fabrication and experimental characterization

The structures demonstrated in this study have been designed as compliant mechanisms in which actuators made from active materials beams were integrated. The use of the compliant paradigm allowed to print the mechanism as one part capable to withstand itself during fabrication. pNIPAM and IP-S were chosen as materials for the actuator and the compliant mechanism respectively. The large deformation of the pNIPAM allows to generate large movement of the structures. The high rigidity and printability of the IP-S allow to make slender yet still robust structures, and shape the material finely to obtain the degrees of freedom of the mechanism.

A 2-step printing process [28] based on a commercial 2PP printer (Photonic Professional GT+, Nanoscribe GmbH) was employed for the fabrication of the bi-material

devices. The compliant mechanism was first printed out of a commercial IP-S resin (IP-S, Nanoscribe GmbH), and then developed. In a second step, the actuators were printed from a custom pNIPAM resin into the previously printed mechanism.

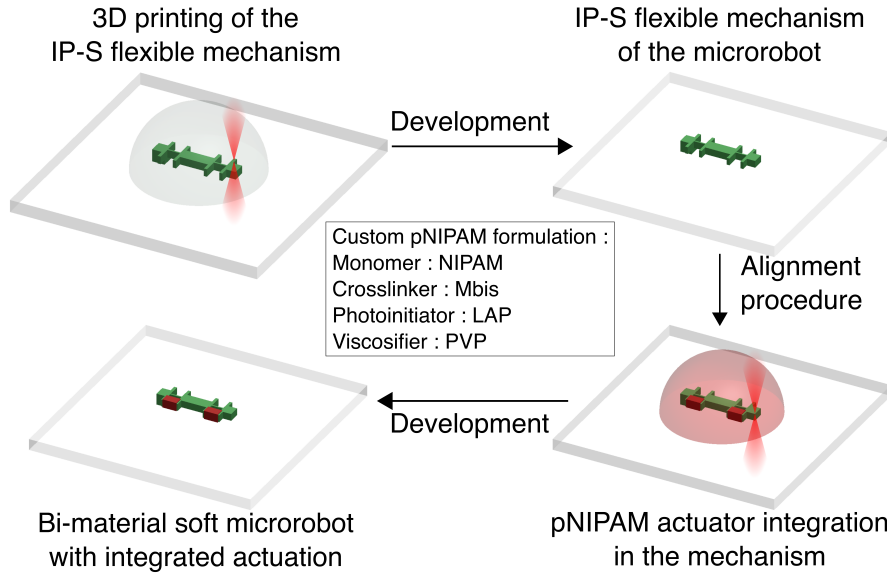


Fig. 2: Fabrication process for IP-S/pNIPAM bi-material microrobots: printing of the IP-S flexible mechanism, development of the IP-S resin, alignment procedure with cross markers, printing of the pNIPAM actuators in the IP-S mechanism, development of the pNIPAM resin.

The displacement characterization was performed experimentally with a heating/cooling plate (Cole-Parmer IC20 C-P) to control temperature. A CMOS camera (Imaging Source DFK 37BUX178) mounted on a microscope (Mitutoyo M Plan Apo. 7.5X/0.21 objective, with an Optem ZOOM 70XL optical tube) was used to acquire images of the devices under heating. Measurements were later extracted from the acquired video via image processing in Matlab.

2.2 Force simulation of the pNIPAM actuators using FEM

A FEM model was used to extrapolate the force that could be generated by the pNIPAM actuator. The pNIPAM was considered as a linear elastic material, while the effect of temperature was taken into account using the phenomenological model proposed by Puleo and al. [29]. The mechanical properties of the pNIPAM were expressed relatively to the swollen state, with the pNIPAM state at $T_0 = 22^\circ\text{C}$ considered as reference. In this model, the contraction $V(T)/V(T_0)$ of the material is modeled with equation (1), with M and m the asymptotic value of the sigmoid function at high and

low temperature respectively, $T_{\text{inflection}}$ the inflection point of the sigmoid and D a parameter tailoring the transition width.

$$\frac{V(T_0)}{V(T)} = M/m + \frac{1 - M/m}{1 + e^{\frac{T - T_{\text{inflection}}}{D}}} \quad (1)$$

From the volumic ratio, the thermal strain ϵ_{th} can be retrieved with equation (2).

$$\frac{V(T_0)}{V(T)} = \frac{1}{(\epsilon_{th} + 1)^3} \quad (2)$$

The evolution of the pNIPAM stiffness, through it's Young's modulus $E(T)$, with respect to the pNIPAM temperature is described by equation (3) [29], [30], with E_0 the Young modulus of the pNIPAM at the reference temperature T_0 and n a specific parameter of the relation between Young's Modulus and the polymer volume ratio.

$$\frac{E(T)}{E(T_0)} = \left(\frac{V(T_0)}{V(T)} \right)^n \quad (3)$$

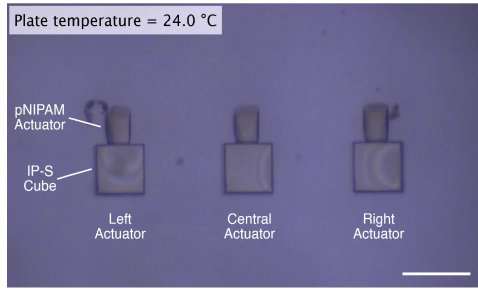
In each force studies, the parameters M/m , $T_{\text{inflection}}$ and D of the constitutive law (1) were fitted on the contraction measurements of the actuators, by calculating in each case the relative volumic ratio $\frac{V(T_0)}{V(T)}$ values calculated with the equation (2). Mechanical measurements of pNIPAM done by Spratte et al. [23] were used to deduce the E_0 and n values, since this study use a similar pNIPAM resin formulation. The contraction measurement done by Spratte et al. were used as matching metric. More details on the methods used can be found in the supplementary materials.

3 STUDY OF THE PNIPAM ACTUATOR STATIC BEHAVIOR

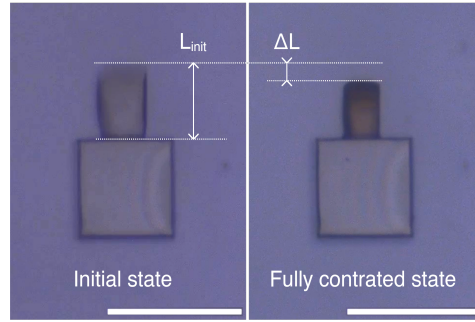
3.1 Free displacement study

The free deformation of the actuator along their length according to temperature was experimentally studied with three $45 \times 30 \times 30 \mu\text{m}$ pNIPAM cantilever beams as actuators, printed on $75 \times 75 \times 75 \mu\text{m}$ IP-S cubes, as depicted in Fig. 3a. A noticeable swelling of the pNIPAM actuators was observed at the end of the actuator printing, with their length reaching $55 \mu\text{m}$ after development.

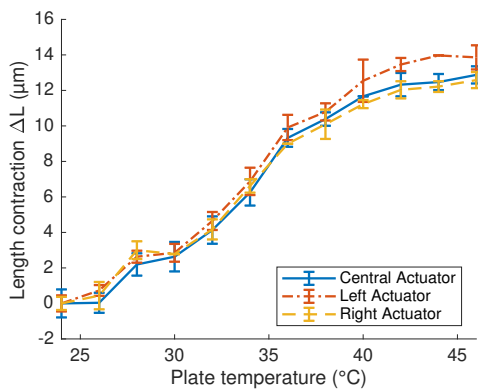
(a)



(b)



(c)



(d)

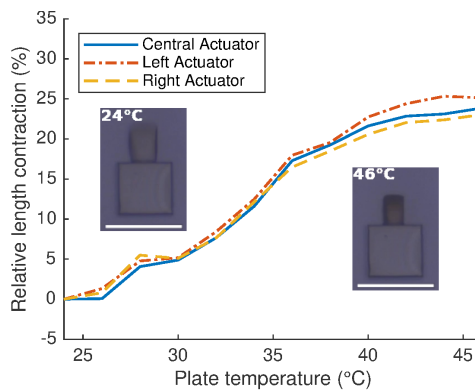


Fig. 3: Experimental measurement of the linear shrinkage of the fabricated pNIPAM actuators. (a) The 3 pNIPAM actuators used for the length contraction measurements presented in (c) and (d). (b) The central pNIPAM actuator depicted in (a) in its initial swelled state (at 24°C) and in its fully contracted state (at 46°C), with a depiction of the measured ΔL length contraction. (c) Length contraction ΔL of each pNIPAM actuator depicted in (a) relative to the heating plate temperature. (d) Relative length contraction $\Delta L/L_{init}$ of the actuators with respect to the heating plate temperature. All scale bars : 100 μm

To measure the shrinkage of the actuators relative to temperature, the three beams were heated between 24°C and 46°C by 2°C steps, each step lasting 5 minutes. At the end of each step, 10 frames were extracted and used to measure the length of each beam (Fig. 3b). A 25% contraction of the beam was observed, following a sigmoidal evolution relative to temperature (Fig. 3c). This is in line with previous work on pNIPAM [20], [21]. The pNIPAM actuator also displayed a linear contraction span

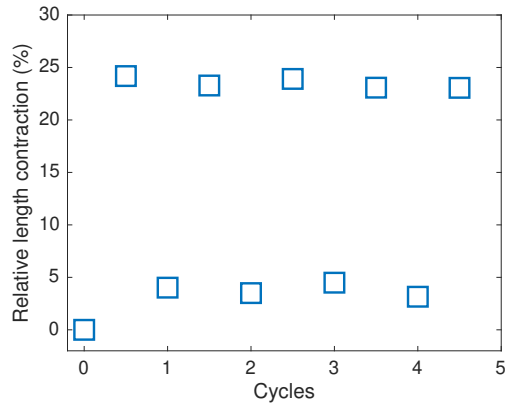


Fig. 4: Contraction of 6 pNIPAM actuators during 5 cycles between 22 and 46°C relatively to their initial length at the beginning of the experiment, with 5 min. of heating/cooling between each point.

between 30°C and 40°C, which could be useful for the accurate position control of a soft microrobot. The repeatability of the pNIPAM actuator was tested with a cycling test carried on 6 $45 \times 30 \times 30 \mu\text{m}$ actuator. Those actuator were submitted to 5 heating and cooling cycles between 22°C and 46°C, with each cycles during 10 minutes (5 minutes of heating between 22 and 46 °C, and 5 minutes of cooling between 46 and 22 °C). A relative length contraction of 24 % was consistently observed across the 5 actuation cycles (Fig. 4), which indicate a good repeatability of the actuation.

3.2 Study of the actuator behavior under load

The behavior of the pNIPAM actuator under load was studied via Finite Element Modelling. The model was first validated in the free displacement case on the two supplementary actuators, since they were not used to fit the model's parameters. The FEM was used to simulate a $55 \times 30 \times 30 \mu\text{m}$ pNIPAM actuator (to take into account the post-print swelling of the actuators) in a cantilever configuration submitted to temperatures between 22°C and 46°C. The simulated length variation was compared to the experimental measurements of two supplementary actuators. The experimental results and the simulated result were in accordance (Online Resource 2). This gives us enough confidence in the model to extrapolate the force behavior of the actuator from it.

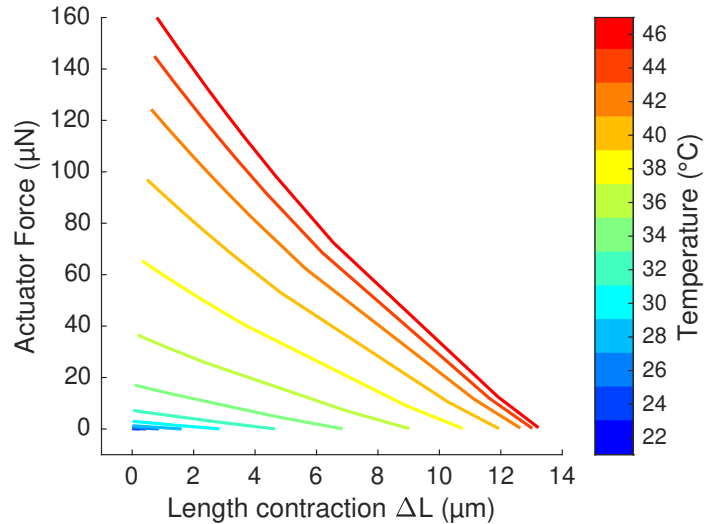


Fig. 5: FEM study of the behavior of a pNIPAM actuator with a spring load applied at one end and no displacement at the other. The figure depicts the Force-displacement relation of the pNIPAM beams in the form of several isotherm curves.

The force-displacement relation of the actuator was then studied, by simulating a $55 \times 30 \times 30 \mu\text{m}$ pNIPAM actuator with a roller boundary condition at one end and a spring load at the other. By varying the spring load stiffness between 0.001 N/m and 201 N/m , the force-displacement curve of the actuator was calculated for several isotherms between 22°C and 46°C (Fig. 5).

The case where the actuator displayed no displacement was also studied to get an idea of the maximum force that can be expected. For this case, a $55 \times 30 \times 30 \mu\text{m}$ pNIPAM actuator with roller boundary condition at both ends to fix the length of the actuator was simulated. The force generated by the actuator was calculated for temperatures between 22°C and 46°C (Online Resource 3).

At 45°C , the model predicts a maximum force of $166 \mu\text{N}$, one order of magnitude higher than the forces reported in the literature for pNIPAM actuators ($10.3 \mu\text{N}$ in [26]) or other hydrogels ($34 \mu\text{N}$ in [27]). However, the values reported in the literature were measured with elastic beam-based protocols (the hydrogel deforms a beam in a passive material supposed elastic, and the displacement is converted into force based on the stiffness of the beam). Since a displacement is present, the measured actuator force in this kind of protocol would be lower according to Fig. 5. Indeed, when the simulated force values of the proposed actuator at 45°C (Fig. 5) are compared to the measure of Özkale et al. [26] for a similar displacement, similar values of force are obtained (respectively $10.3 \mu\text{N}$ for a 20% displacement and $12 \mu\text{N}$ for a 21% displacement). These results show an interesting behavior of the pNIPAM actuator in force: the actuator can be very delicate if allowed to move, but with one order of

magnitude greater forces under its belt. This extra push could facilitate various tasks, by overpowering perturbing forces like drag forces of faster fluid flows or cells adhesion to a substrate [31]. It could also allow to do new tasks, like yeast crushing [32]

3.3 Effect of the printing speed on the pNIPAM actuator’s behavior

To study the effect of the printing speed on the pNIPAM actuator’s behavior, 3 sets of $3 \times 55 \times 30 \mu\text{m}$ pNIPAM actuators were printed. The printing speed was set for each set at 20, 40 or 60 mm/s respectively while the other printing parameters were left unchanged.

Following the same protocol as before, the free contraction of each actuator was measured. The parameters M/m , $T_{inflection}$ and D of the pNIPAM model were then fitted on those measurements for each printing speed. We had a coefficient of determination R^2 of 0.9884, 0.9742 and 0.9286 for the 20, 40 and 60 mm/s fit respectively, and the obtained models fit experimental observations in the free contraction case (Fig. 6a). The E_0 and n parameters were then set based on the measurements proposed in Spratte et al. [23], using the contraction measured experimentally and those reported by [23] as the matching metric.

Table 1: Parameters used in the FEM model of the pNIPAM actuator for each printing speed.

Speed	M/m	$T_{inflection}$	D	E_0	n
20k	2.3	30 °C	2.5 °C	19 kPa	2.89
40k	3.2	31.7 °C	2 °C	8.5 kPa	2.28
60k	3.4	33.5 °C	1.6 °C	5 kPa	1.99

Fig. 6a and Table 1 show the impact of the printing speed of the pNIPAM actuator on their free contraction. The maximal length contraction increase from 13 to 18 μm between actuators printed at a 20 and 60 mm/s printing speed, but no significant change of maximum contraction is observed between actuators printed at 40 and 60 mm/s. The transition temperature of the actuator rise by a few degrees when the printing speed increase, while the transition range narrows (Table 1). A detail worth noting is that the n parameter of the model decrease from 3 to 2 as the printing speed increase. According to the Flory theory of swelled polymers [33] [29], a polymer swelled in a good solvent should have a parameter $n = 2$ if its crosslinking is low. Thus, the decrease of the polymer’s crosslinking caused by the increase of the printing speed could explain the observed decrease of the n parameter.

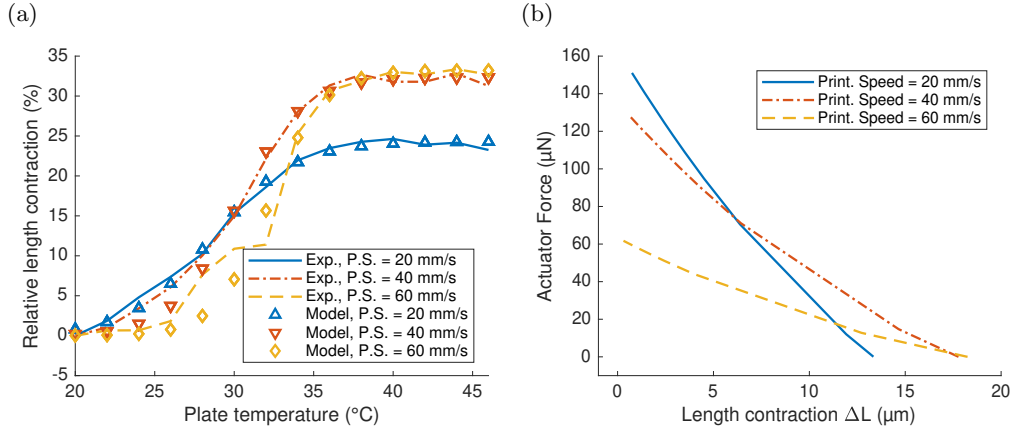


Fig. 6: (a) Experimental measurement of the relative length contraction with respect to the temperature on pNIPAM actuators made with various printing speed (20 mm/s, 40 mm/s, and 60 mm/s), compared to the theoretical length contraction predicted by the FEM model. (b) Force-displacement isocurve of a pNIPAM actuator with a printing speed of 20 mm/s, 40 mm/s, and 60 mm/s respectively, obtained via FEM.

From those models, the static behavior of pNIPAM actuators at different printing speed was studied with FEM in a spring-load configuration (Fig. 6b), as done in the previous subsection. When submitted to a spring load ranging from 0.001 N/m to 201 N/m, the simulation showed a force range of 151-0 μN , 128-0 μN and 62-0 μN for the actuators printed with a printing speed of 20 mm/s, 40 mm/s and 60 mm/s respectively. The associated length contraction range is 0 to 13 μm , 0 to 18 μm and 0 to 18 μm . Of the 3 printing speed tested, the pNIPAM actuator printed with a 40 mm/s printing speed is the best compromise between the force and displacement generated, showing a 15% reduction of the maximal force range while augmenting by 28% the length contraction range. Moreover, we can observe that the actuator printed at 60 mm/s printing speed doesn't improve either the force or the displacement obtained compared to the actuator printed at 40 mm/s. However, it should be noted that using the 60 mm/s actuator allow to obtain the best force resolution in the 0-60 μN range for a same temperature range.

4 BEHAVIOR OF IP-S/pNIPAM BIMATERIAL MECHANISMS UNDER THERMAL ACTUATION

4.1 Movement of bi-material rotational beam joints under actuation

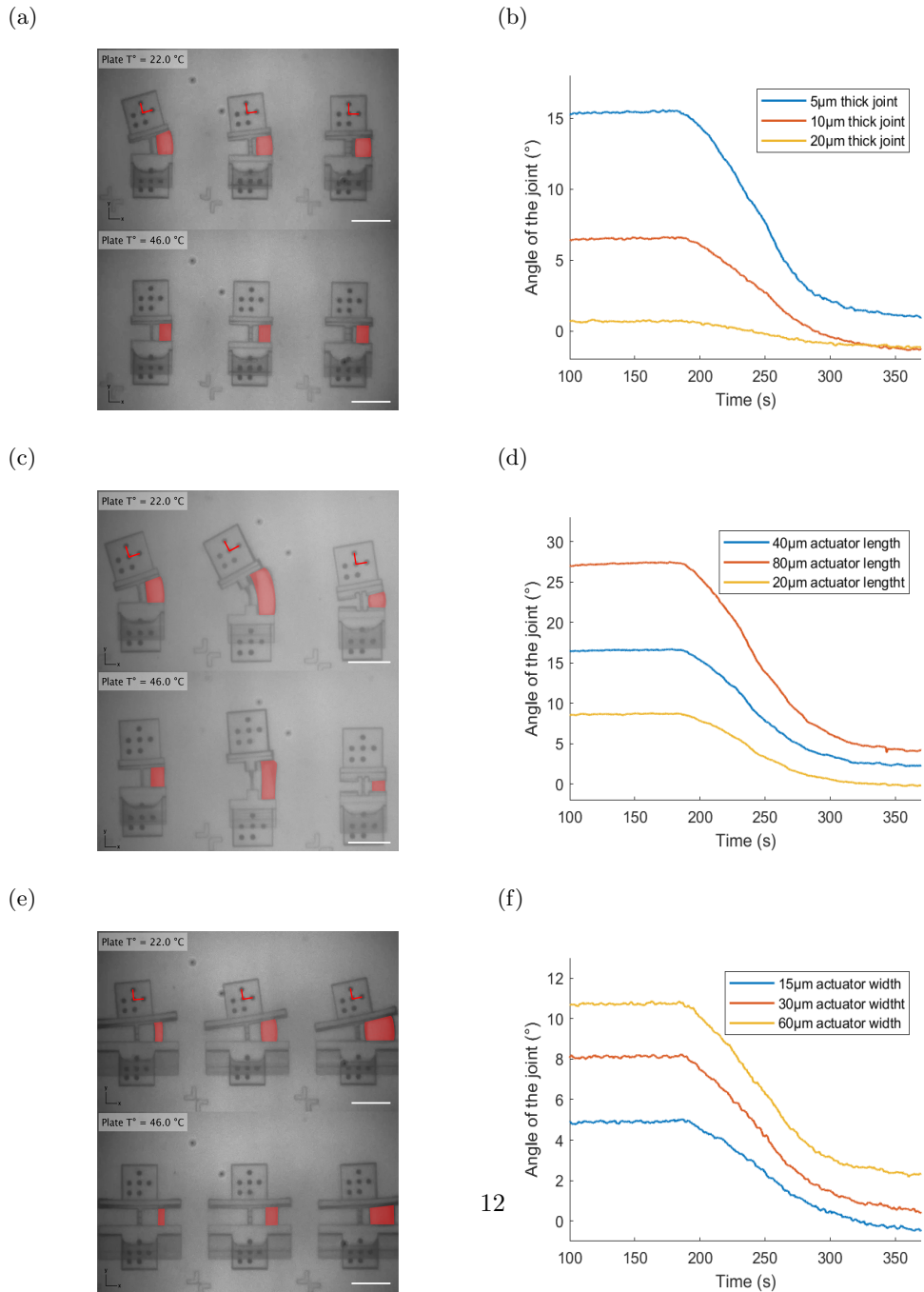


Fig. 7: Study of the movement of different link-actuator configuration according to three parameters : (a), (b) Joint stiffness vs its thickness, (c), (d) Actuator length, and (e), (f) actuator width. The actuators are highlighted in red. Scale bars: 100 μm .

The angular movement under actuation of bi-material rotational beam joints was studied (Fig. 7) under heating between 22 and 46 °C, relatively to three parameters : the stiffness of the compliant joint, the length and the width of the actuator. In the stiffness variation test, a $45 \times 30 \times 30 \mu\text{m}$ pNIPAM actuators was used to actuate 3 joints of length $40 \mu\text{m}$ and width $25 \mu\text{m}$. The stiffness of the joint was tuned by it's thickness, between 5, 10 and $20 \mu\text{m}$, and 6 samples of each configuration. In the length variation test, a $40 \times 25 \times 5 \mu\text{m}$ beam joint was used, actuated by a $30 \times 30 \mu\text{m}$ pNIPAM actuator, with the length of the actuator tuned between 20, 40 and $80 \mu\text{m}$, and 5 samples of each configuration.. In the width variation test, a $40 \times 25 \times 10 \mu\text{m}$ beam joint was used, actuated by a $40 \times 30 \mu\text{m}$ pNIPAM actuator, with the width of the actuator tuned between 15, 30, and $60 \mu\text{m}$, and 6 samples of each configuration.

When the joint stiffness was swept (Fig. 7b, Sup. Table 2), a cubic variation of the angular displacement relatively to the joint thickness is observed between the $20 \mu\text{m}$ and $10 \mu\text{m}$ thick joints (as we could expect, since the joint stiffness and thickness are related in a cubic fashion [34]), but not between the $10 \mu\text{m}$ and $5 \mu\text{m}$ thick joints. In this case, the joint displacement seems to be limited by the maximal contraction of the actuator: with a 25% maximum contraction, the maximum angular displacement that could be generated in a free movement case is 16° with a $40 \mu\text{m}$ long actuator. When the width of the actuator was studied (Fig. 7f, Sup. Table 4), an augmentation of the angular displacement was observed related to the width of the actuator. However, this augmentation was very subtle between the $30 \mu\text{m}$ and $60 \mu\text{m}$ wide actuators. A linear correlation was observed between angular displacement and actuator length (Fig. 7d, Sup. Table 3). Across all the joints, a maximal angular displacement of 23° was measured with the $80 \mu\text{m}$ long actuator (Fig. 7d).

4.2 Bi-material printing for soft microrobot: a RR serial architecture

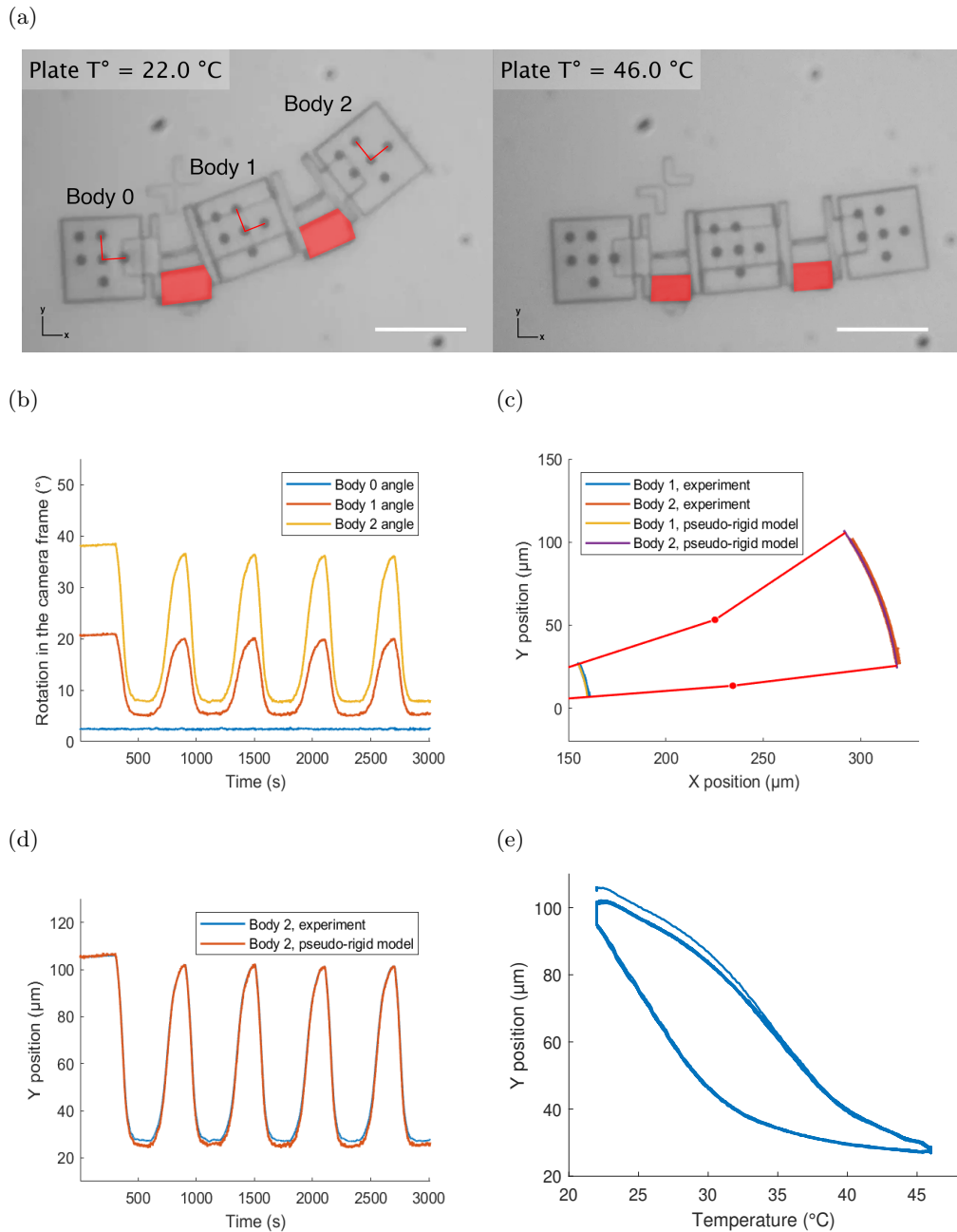


Fig. 8: Study of an RR soft microrobot behavior under global heating. (a) RR microrobot at 22°C and 46°C , with the pNIPAM actuators highlighted in red, Scale bar: $100 \mu\text{m}$. (b) Measured angles of the body 0, 1 and 2, relatively to the camera frame (c) Measured displacement of the bodies 1 and 2 in the XY plane, compared to an equivalent pseudo-rigid model of the RR mechanism. (d) Measured position of the body 2 in Y relatively to time, compared to the RR pseudo-rigid model in the same configuration. (e) Measured position of the body 2 in Y relative to the heating plate temperature. All the XY coordinates reported in (c), (d) and (e) are expressed in the frame of body 0.

A RR soft microrobot design (classic robot design with two revolute joints in series) is proposed to demonstrate the potential of bi-material 2PP printing to make microrobots able of controllable and repeatable movement. The design is composed of three "bodies" (a base attached to the glass substrate and two moving bodies, with tracking markers on each) with two $40 \times 25 \times 5 \mu\text{m}$ beams joint acting as revolute joints and two $45 \times 30 \times 30 \mu\text{m}$ pNIPAM actuators. It was fabricated following the proposed approach. The behavior of the mechanism was investigated under 5 heating/cooling cycles between 22 and 46°C, with 5 min for each temperature at each cycle. The results are shown in Fig. 8a.

A displacement of 83 μm was effected by the body 2 of the RR (Fig. 8c). When compared to a pseudo-rigid model of the RR mechanism (feed with the measured angles of each bodies (Fig. 8b)), the measured movement of the bi-material RR microrobot bodies closely matched (Fig. 8c and 8d), with a max difference of 1.8 μm (the dispersion of the position measurement at 95 % is $\pm 0.41 \mu\text{m}$). Moreover, a good repeatability of the movement across the 5 cycles can be observed (Fig. 8d), with a good controllability relatively to the temperature of the heating element (Fig. 8e).

4.3 3D bi-material 100 μm grippers

As a demonstration of the 3D capability of the fabrication approach, 3 designs of 100 μm 3D grippers (Fig. 9a, d and g) with different integrated actuators (one per finger) are proposed: a flat gripper rotated 45° around one axis, a flat gripper rotated 45° around two axis **[KR]: dire l'angle**, and a 3-jaw mandrel-like gripper ($40 \times 25 \times 5 \mu\text{m}$ beams joint were used with $45 \times 30 \mu\text{m}$ pNIPAM actuators). All the designs are conveniently obtained after the fabrication process and observed under an optical microscope. The heating of the microgrippers between 22°C and 46°C confirmed their capacity to be actuated as shown in Fig. 9b, c, e, f, h, and i, with an initial gap estimated with ImageJ around 25 μm for Fig. 9b and a full closure of all the grippers.

4.4 Discussion

While the mechanisms presented above show great potential for 3D movement and manipulator miniaturization, their actuation is still controlled globally. To make true Multi-DoF micromanipulators from those devices, the capacity to select which actuator will be heated (thus actuated) and the control of the produced temperature is mandatory. Photothermal doping like dyes [35] or nanoparticles [36] could be used in the actuator to convert light into heat, thus triggering the actuator. In this case, the actuation of a specific actuator could be done either via focalized light (under a microscope or an optical tweezer) or by rendering the photothermal conversion selective to a certain wavelength (using orthogonal dyes [35] in the different actuators). Another way to have localized heat could be to integrate electric heaters in close vicinity of the actuators [37], a strategy that could be well suited in microfluidic

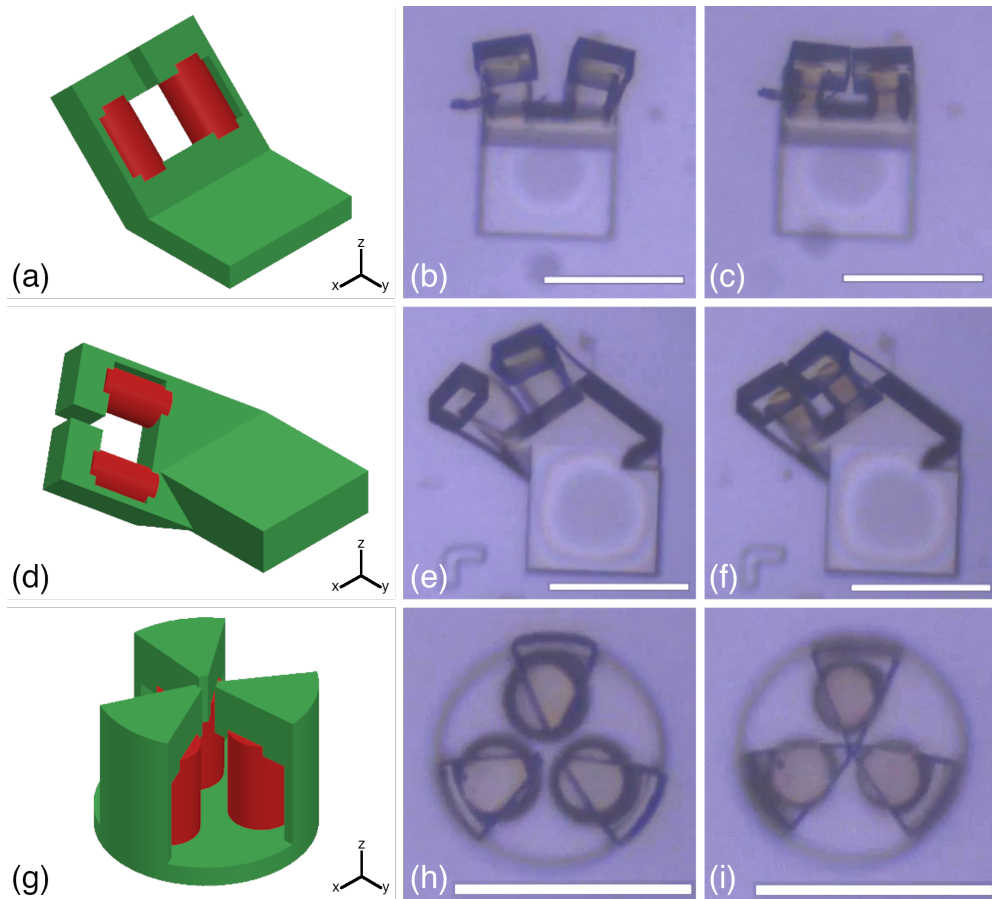


Fig. 9: 3D grippers CAD and their actuation at 22°C and 46°C respectively. In the CAD, the IP-S flexible mechanism is in green and the pNIPAM actuators are in red. (a), (b) and (c) Flat gripper rotated around one axis. (d), (e) and (f) Flat gripper rotated around two axis. (g), (h), (i) 3-jaw mandrel-like gripper. All scale bars are 100 μm .

devices. With this lock lifted, many applications could be considered. Those miniaturized manipulators could be integrated into smaller devices. We could think of a micromanipulator placed at the tip of an optical fiber, which could be brought in-vivo via a catheter and operate biopsy or surgery tasks; or we could envisage the integration of several manipulator inside a microfluidic device, and make an integrated chain for cell bioengineering or In-Vitro Fertilization.

5 CONCLUSION AND PERSPECTIVES

Bi-material 3D printed soft microrobots are proposed in this work, combining flexible mechanisms made from IP-S with integrated actuators made from pNIPAM. A static characterization of pNIPAM as an actuator was performed in free displacement via experimentation and under load via Finite Element Modelling. The effect of a change in the actuator printing speed on its behavior was also investigated. **Across all the fabricated pNIPAM actuators, a maximum relative contraction of 30% was measured, and a maximum blocking force of 166 μN was shown by the FEM simulation. The movement of several beam joints actuated with pNIPAM beams was characterized relatively to the joint stiffness, actuator length, and width, showing a 23° maximal rotation range when varying the temperature in a restrained range (22°C to 46°C).** A RR bi-material soft microrobot was designed and fabricated to study the behavior of multi-material 3D-printed soft microrobots, **and demonstrated a repeatable displacement of 80 μm at its extremity.** The bi-material manufacturing of the IP-S mechanism and pNIPAM actuators was then demonstrated on 3 designs of 3D microgrippers. The closing of each gripper is observed when the temperature is controlled between 22°C and 46°C. The pNIPAM actuators showed promising behavior in force during the finite element analysis, which should be confirmed by further experimental validation. The bi-material strategy could be used with different combinations of passive and active polymers with various stimuli. The proposed approach is an interesting base to make multi-DoF microrobots in the future, and paves the way to achieve complex 3D soft microrobots with large motions and an easily controllable actuation.

Declarations

Funding: This work was supported by the regional Bourgogne Franche-Comté project NanoFolding, the EIPHI Graduate School (contract “ANR-17-EURE-0002”), the French RENATECH network through its FEMTO-ST technological facility, French ROBOTEX network (TIRREX ANR-21-ESRE-0015) through its FEMTO-ST technological facility CMNR and the ANR PNanoBot (contract “ANR-21-CE33-0015”).

Competing Interests: The authors have no relevant financial or nonfinancial interests to disclose.

Consent for publication: All the author’s approved the publication of this work. The copyrights permissions were obtained for all pre-published materials.

Availability of Data and Materials: Not Applicable.

Author’s Contributions: Yannis Bordes, Adam Chafai and Pierre Lambert undertook the first investigations on the pNIPAM formulation. Vincent Luzet and Mehdi Salah stabilized the pNIPAM formulation, and prepared the pNIPAM resin for TPP printing. Gwenn Ulliac and Mehdi Salah prepared the printing process and printed the samples used in this work. Muamer Kadic and Mehdi Salah carried the Finite Element Modelling. Kanty Rabenoroso, Cédric Clévy and Mehdi Salah provided original ideas and took care of designing and analyzing the results of the experiments. Kanty Rabenoroso and Cédric Clévy supervised this work. Pierre Lambert, Muamer Kadic,

Cédric Clévy, and Kanty Rabenorosoa contributed to the conceptualization of the idea and the elaboration of research plan. Kanty Rabenorosoa acquired the fundings for this work. Mehdi Salah carried the experiments and wrote the first draft of the manuscript. All authors provided critical feedback and helped shape the research, analysis, and manuscript.

References

- [1] Sakamoto, K., Aoyama, T., Takeuchi, M., Hasegawa, Y.: Intuitive Cell Manipulation Microscope System with Haptic Device for Intracytoplasmic Sperm Injection Simplification. *Sensors* **24**(2), 711 (2024) <https://doi.org/10.3390/s24020711>
- [2] Saketi, P., Von Essen, M., Mikczinski, M., Heinemann, S., Fatikow, S., Kallio, P.: A flexible microrobotic platform for handling microscale specimens of fibrous materials for microscopic studies. *Journal of Microscopy* **248**(2), 163–171 (2012) <https://doi.org/10.1111/j.1365-2818.2012.03660.x>
- [3] Snyder, B., Corbett, B., O'Brien, P.: Hybrid integration of the wavelength-tunable laser with a silicon photonic integrated circuit. *Journal of Lightwave Technology* **31**(24), 3934–3942 (2013) <https://doi.org/10.1109/JLT.2013.2276740>
- [4] Chevallier, A., Akleh, W., Govilas, J., Boutenel, F., Guicheret-Retel, V., Beau-grand, J., Clévy, C., Placet, V.: Moisture effects on the transverse compressive behaviour of single flax fibres. *Composites Part A: Applied Science and Manufacturing* **188**, 108509 (2025) <https://doi.org/10.1016/j.compositesa.2024.108509>
- [5] Lamont, S., Fropier, J., Abadie, J., Piat, E., Constantinescu, A., Roux, C., Vernerey, F.: Profiling oocytes with neural networks from images and mechanical data. *Journal of the Mechanical Behavior of Biomedical Materials* **138**, 105640 (2023) <https://doi.org/10.1016/j.jmbbm.2022.105640>
- [6] McClintock, H., Temel, F.Z., Doshi, N., Koh, J.-s., Wood, R.J.: The milliDelta: A high-bandwidth, high-precision, millimeter-scale Delta robot. *Science Robotics* **3**(14), 3018 (2018) <https://doi.org/10.1126/scirobotics.aar3018>
- [7] Leveziel, M., Haouas, W., Laurent, G.J., Gauthier, M., Dahmouche, R.: MiGri-Bot: A miniature parallel robot with integrated gripping for high-throughput micromanipulation. *Science Robotics* **7**(69), 4292 (2022) <https://doi.org/10.1126/scirobotics.abn4292>
- [8] Nwafor, C., Laurent, G.J., Rabenorosoa, K.: Miniature parallel continuum robot made of glass: Analysis, design, and proof-of-concept. *IEEE/ASME Transactions on Mechatronics* **28**(4), 2038–2046 (2023) <https://doi.org/10.1109/TMECH.2023.3276230>
- [9] Xing, Z., Zhang, J., McCoul, D., Cui, Y., Sun, L., Zhao, J.: A Super-Lightweight

- and Soft Manipulator Driven by Dielectric Elastomers. *Soft Robotics* **7**(4), 512–520 (2020) <https://doi.org/10.1089/soro.2018.0134>
- [10] Yang, S.H., Kim, Y.-S., Yoo, J.-M., Dagalakis, N.G.: Microelectromechanical systems based Stewart platform with sub-nano resolution. *Applied Physics Letters* **101**(6), 061909 (2012) <https://doi.org/10.1063/1.4739517>
- [11] Balucani, M., Belfiore, N., Crescenzi, R., Verotti, M.: The development of a MEMS/NEMS-based 3 D.O.F. compliant micro robot. *International Journal of Mechanics and Control* **12**, 3–10 (2011) <https://doi.org/10.1109/RAAD.2010.5524590>
- [12] Benouhiba, A., Wurtz, L., Rauch, J.-Y., Agnus, J., Rabenoroso, K., Clévy, C.: Nanorobotic structures with embedded actuation via ion induced folding. *Advanced Materials* **33**(45), 2103371 (2021) <https://doi.org/10.1002/adma.202103371>
- [13] Kawata, S., Sun, H.-B., Tanaka, T., Takada, K.: Finer features for functional microdevices. *Nature* **412**(6848), 697–698 (2001) <https://doi.org/10.1038/35089130>
- [14] Mainik, P., Spiegel, C.A., Blasco, E.: Recent Advances in Multi-Photon 3D Laser Printing: Active Materials and Applications. *Advanced Materials* **36**(11), 2310100 (2024) <https://doi.org/10.1002/adma.202310100>
- [15] Adam, G., Benouhiba, A., Rabenoroso, K., Clévy, C., Cappelleri, D.J.: 4D Printing: Enabling Technology for Microrobotics Applications. *Advanced Intelligent Systems* **3**(5), 2000216 (2021) <https://doi.org/10.1002/aisy.202000216>
- [16] Curie, P.: Sur la symétrie dans les phénomènes physiques, symétrie d’un champ électrique et d’un champ magnétique. *Journal de Physique Théorique et Appliquée* **3**(1), 393–415 (1894) <https://doi.org/10.1051/jphysap:018940030039300>
- [17] Jin, D., Chen, Q., Huang, T.-Y., Huang, J., Zhang, L., Duan, H.: Four-dimensional direct laser writing of reconfigurable compound micromachines. *Materials Today* **32**, 19–25 (2020) <https://doi.org/10.1016/j.mattod.2019.06.002>
- [18] Huang, T.-Y., Huang, H.-W., Jin, D.D., Chen, Q.Y., Huang, J.Y., Zhang, L., Duan, H.L.: Four-dimensional micro-building blocks. *Science Advances* **6**(3), 8219 (2020) <https://doi.org/10.1126/sciadv.aav8219>
- [19] Hippler, M., Blasco, E., Qu, J., Tanaka, M., Barner-Kowollik, C., Wegener, M., Bastmeyer, M.: Controlling the shape of 3D microstructures by temperature and light. *Nature Communications* **10**(1), 232 (2019) <https://doi.org/10.1038/s41467-018-08175-w>

- [20] Decroly, G., Chafai, A., Timary, G., Gandolfo, G., Delchambre, A., Lambert, P.: A Voxel-Based Approach for the Generation of Advanced Kinematics at the Microscale. *Advanced Intelligent Systems* **5**(7), 2200394 (2023) <https://doi.org/10.1002/aisy.202200394>
- [21] Deng, C., Liu, Y., Fan, X., Jiao, B., Zhang, Z., Zhang, M., Chen, F., Gao, H., Deng, L., Xiong, W.: Femtosecond Laser 4D Printing of Light-Driven Intelligent Micromachines. *Advanced Functional Materials* **33**(11), 2211473 (2023) <https://doi.org/10.1002/adfm.202211473>
- [22] Lee, M.R., Phang, I.Y., Cui, Y., Lee, Y.H., Ling, X.Y.: Shape-Shifting 3D Protein Microstructures with Programmable Directionality via Quantitative Nanoscale Stiffness Modulation. *Small* **11**(6), 740–748 (2015) <https://doi.org/10.1002/sml.201401343>
- [23] Spratte, T., Geiger, S., Colombo, F., Mishra, A., Taale, M., Hsu, L.-Y., Blasco, E., Selhuber-Unkel, C.: Increasing the Efficiency of Thermoresponsive Actuation at the Microscale by Direct Laser Writing of pNIPAM. *Advanced Materials Technologies* **8**(1), 2200714 (2023) <https://doi.org/10.1002/admt.202200714>
- [24] Nishiguchi, A., Mourran, A., Zhang, H., Möller, M.: In-Gel Direct Laser Writing for 3D-Designed Hydrogel Composites That Undergo Complex Self-Shaping. *Advanced Science* **5**(1), 1700038 (2018) <https://doi.org/10.1002/advs.201700038>
- [25] Zhang, M., Pal, A., Zheng, Z., Gardi, G., Yildiz, E., Sitti, M.: Hydrogel muscles powering reconfigurable micro-metastructures with wide-spectrum programmability. *Nature Materials* **22**(10), 1243–1252 (2023) <https://doi.org/10.1038/s41563-023-01649-3>
- [26] Özkale, B., Parreira, R., Bekdemir, A., Pancaldi, L., Özelçi, E., Amadio, C., Kaynak, M., Stellacci, F., Mooney, D.J., Sakar, M.S.: Modular soft robotic microdevices for dexterous biomanipulation. *Lab on a Chip* **19**(5), 778–788 (2019) <https://doi.org/10.1039/C8LC01200H>
- [27] Ma, Z.-C., Zhang, Y.-L., Han, B., Hu, X.-Y., Li, C.-H., Chen, Q.-D., Sun, H.-B.: Femtosecond laser programmed artificial musculoskeletal systems. *Nature Communications* **11**(1), 4536 (2020) <https://doi.org/10.1038/s41467-020-18117-0>
- [28] Lee, Y., Kim, J., Bozuyuk, U., Dogan, N.O., Khan, M.T.A., Shiva, A., Wild, A., Sitti, M.: Multifunctional 3D-Printed Pollen Grain-Inspired Hydrogel Micro-robots for On-Demand Anchoring and Cargo Delivery. *Advanced Materials* **35**(10), 2209812 (2023) <https://doi.org/10.1002/adma.202209812>
- [29] Puleo, G.L., Zulli, F., Piovanelli, M., Giordano, M., Mazzolai, B., Beccai, L., Andreozzi, L.: Mechanical and rheological behavior of pNIPAAm crosslinked macrohydrogel. *Reactive and Functional Polymers* **73**(9), 1306–1318 (2013) <https://doi.org/10.1016/j.reactfunctpolym.2013.07.004>

- [30] Anseth, K.S., Bowman, C.N., Brannon-Peppas, L.: Mechanical properties of hydrogels and their experimental determination. *Biomaterials* **17**(17), 1647–1657 (1996) [https://doi.org/10.1016/0142-9612\(96\)87644-7](https://doi.org/10.1016/0142-9612(96)87644-7)
- [31] Köser, J., Gaiser, S., Müller, B.: Contractile cell forces exerted on rigid substrates. *European Cells & Materials* **21**, 479–486486487 (2011) <https://doi.org/10.22203/ecm.v021a36>
- [32] Stenson, J.D., Hartley, P., Wang, C., Thomas, C.R.: Determining the mechanical properties of yeast cell walls. *Biotechnology Progress* **27**(2), 505–512 (2011) <https://doi.org/10.1002/btpr.554>
- [33] Flory, P.J.: *Principles Of Polymer Chemistry*. Cornell University Press, Ithaca, New York (1953)
- [34] Henein, S.: *Conception des structures articulées à guidages flexibles de haute précision*. PhD thesis, EPFL, Lausanne (2000). <https://doi.org/10.5075/epfl-thesis-2194>
- [35] Hsu, L.-Y., Mainik, P., Münchinger, A., Lindenthal, S., Spratte, T., Welle, A., Zaumseil, J., Selhuber-Unkel, C., Wegener, M., Blasco, E.: A Facile Approach for 4D Microprinting of Multi-Photoresponsive Actuators. *Advanced Materials Technologies* **8**(1), 2200801 (2022) <https://doi.org/10.1002/admt.202200801>
- [36] Xin, C., Ren, Z., Zhang, L., Yang, L., Wang, D., Hu, Y., Li, J., Chu, J., Zhang, L., Wu, D.: Light-triggered multi-joint microactuator fabricated by two-in-one femtosecond laser writing. *Nature Communications* **14**(1), 4273 (2023) <https://doi.org/10.1038/s41467-023-40038-x>
- [37] Cao, Y., Dong, J.: High-performance low-voltage soft electrothermal actuator with directly printed micro-heater. *Sensors and Actuators A: Physical* **297**, 111546 (2019) <https://doi.org/10.1016/j.sna.2019.111546>